The Journal of Chemical Physics

Stability of oxidized states of free-standing and ceria-supported PtO_x particles

Cite as: J. Chem. Phys. (in press) (2022); https://doi.org/10.1063/5.0099927
Submitted: 19 May 2022 • Accepted: 25 July 2022 • Accepted Manuscript Online: 25 July 2022

Jon Eunan Quinlivan Domínguez, Konstantin M. Neyman and Albert Bruix

Accepted to J. Chem. Phys. 10.1063/5.0099927

Stability of oxidized states of free-standing and ceria-supported PtO_x particles

Jon Eunan Quinlivan Domínguez,[1] Konstantin M. Neyman,[1,2] Albert Bruix[1,*]

[1]*Departament de Ciència de Materials i Química Física and Institut de Química Teòrica i Computacional (IQTCUB), Universitat de Barcelona, 08028, Barcelona, Spain*

[2]*ICREA (Institució Catalana de Recerca i Estudis Avançats), 08010, Barcelona, Spain*

*corresponding author: abruix@ub.edu

ABSTRACT: Nanostructured materials based on CeO_2 and Pt play a fundamental role in catalyst design. However, their characterization is often challenging due to their structural complexity and the tendency of the materials to change under reaction conditions. In this work, we combine calculations based on the density functional theory, a machine-learning assisted global optimization method (GOFEE), and *ab initio* thermodynamics to characterize stable oxidation states of ceria-supported Pt_yO_x particles in different environments. The collection of global minima structures for different stoichiometries resulting from the global optimisation effort is used to assess the effect of temperature, oxygen pressure, and support interactions on the phase diagrams, oxidation states, and geometries of the Pt_yO_x particles. We thus identify favoured structural motifs and O:Pt ratios, revealing that oxidized states of free-standing and ceria-supported platinum particles are more stable than reduced ones under a wide range of conditions. These results indicate that studies rationalizing activity of ceria-supported Pt clusters must consider oxidized states, and that previous understanding of such materials obtained only with fully reduced Pt clusters may be incomplete.

1. INTRODUCTION

Nanostructured materials based on ceria (CeO_2) and Pt have a wide range of applications in catalysis, such as the three-way conversion of automobile exhausts,[1] anode[2] or cathode[3] materials of fuel cells, or mediating the water gas shift reaction,[4,5] among others.[6] CeO_2 is typically used in such materials as a non-inert support for the more active Pt phase, leading to intricate metal-support interactions that affect the electronic structure and chemical properties of both the metal and the oxide.[7–9] These electronic metal-support interactions further complicate the already challenging task of characterizing the properties of nanostructured catalytic materials, which are typically structurally complex. Their size, structure, and oxidation state not only depend on preparation conditions, but also often undergo significant transformations under reaction conditions, as revealed by *in situ* or *operando* spectroscopic techniques.[10–12] These structural and environmental complexities therefore hinder the straightforward computational modelling of working heterogeneous catalysts by means of first principles-based approaches.[13,14]

In catalysts based on Pt and ceria, Pt is present as nano- or subnano-particles of varying size,[15–17] or as single atoms, either anchored to the ceria surface[2,18–20] or inserted in the ceria lattice.[21–23] Atomically dispersed Pt on ceria substrates has been studied extensively by means of combined experimental and computational approaches during the last decade because single-atom Pt centres allow to significantly increase specific activity for different reactions.[2,19,24] In such composites, Pt is often found in a cationic form (i.e. Pt^{n+} species with n= 1, 2, or 4) either occupying Ce positions of the ceria lattice or deposited on under-coordinated surface sites of ceria. The oxidation state of Pt atoms depends on their coordination environment and on the stoichiometry of ceria substrate, which can either accept or donate electrons by varying the occupation of the Ce4f states (reducing Ce^{4+} cations to Ce^{3+} and *vice versa*) and/or the amount of O in the ceria lattice.

Atomically dispersed Pt has often been distinguished from metallic nano- or subnano- Pt particles by the characteristic shifts of cationic Pt in X-Ray Photoemission Spectroscopy (XPS).[2,18,25,26] Nevertheless, recent studies report the formation of small oxidized Pt particles (i.e. PtO_x) under reaction conditions and suggest a relevant role of Pt-O-Pt motifs in activating oxidation reactions.[25,27,28] The interplay between stability, structure, and oxidation state of such ceria-supported PtO_x particles is however not well understood. In fact, during the last two decades, most studies modelling ceria-supported

Pt particles have considered only non-oxidized states of Pt particles.[5,7,29,30] In addition, the majority of the aforementioned models (with notable exceptions)[27] were constructed by rather heuristic trial and error approaches, instead of using automated and unbiased global optimization or sampling approaches, which would ensure that the constructed models correspond to stable structures of the represented systems.

The use of sampling methods based on Monte Carlo approaches or of global optimization methods such as evolutionary algorithms have now been available for years and applied quite successfully to determine the structure of supported metal or oxide clusters.[27,31–37] Of particular interest to characterizing the oxidation states of supported metal clusters are approaches that combine global optimization of various stoichiometries with a subsequent thermodynamic analysis,[35,38,39] or those that directly sample structure and stoichiometries under given conditions using grand canonical approaches.[27,32] The resulting phase-diagrams allow to pinpoint states stable under given conditions, relying on well-defined structural models.

In order to identify the stable structures and oxidation states of ceria-supported Pt particles, we therefore combine a novel global optimization method with *ab initio* thermodynamics. We focus on the characterization of prevailing structural motifs, the effects of conditions on the stability of different oxidation states, and the role of the ceria support. In particular, we use a machine-learning assisted algorithm for the exploration of the configurational space.[40] Once the most stable structures have been determined for the targeted stoichiometries, their Gibbs free energy of formation is evaluated under varying conditions by means of *ab initio* thermodynamics (AITD).[41,42] A consistent picture emerges for the formation and oxidation of both free-standing and ceria-supported PtO_x particles, revealing support effects on the structural and compositional properties of PtO_x clusters, and the changes induced by exposure to different environmental conditions. Oxidized states of PtO_x clusters are found to be prevalent under a wide range of reaction conditions.

2. METHODS AND COMPUTATIONAL DETAILS

We carry out a systematic global optimization study based on density functional theory (DFT) calculations and the "global optimization with first-principles energy expression (GOFEE)"[40] method to elucidate the stability of PtO_x clusters with varying

oxygen content under different conditions, the effects of particle size and a $CeO_2(111)$ support, and the overall electronic structure of these systems. We target Pt_yO_x clusters with y = 3 or 6 and x = 0 – 2y. Both free-standing and $CeO_2(111)$-supported structures are evaluated. For the $CeO_2(111)$-supported structures, only the supported particles are globally optimized, whereas the atoms of the CeO_2 surface are kept in their bulk-terminated positions. The structural characterization of each targeted stoichiometry consists in obtaining the configuration with the lowest internal energy, i.e. the (putative) Global Minimum (GM). Once the GM has been determined for all the considered stoichiometries of the system, AITD is used to evaluate the free energies of each stoichiometry and to generate the corresponding phase diagrams. In this section, we describe the global optimization strategy using GOFEE, the DFT calculations, and the AITD approach used.

2.1. GOFEE method and global optimization strategy

The GOFEE method allows to reduce the number of energy and force evaluations carried out at the theory level of choice by training, on-the-fly, a surrogate machine-learning energy model. This model is used to carry out local relaxations of every evaluated candidate structure and to guide the exploration of conformational space, which supposes a considerable improvement in computational efficiency with respect to other algorithms.[31,37] The GOFEE code therefore relies on a selected number of single-point calculations, circumventing the need for performing more demanding local relaxations at commonly quite costly levels of theory.

For each stoichiometry under scrutiny, the method employs the following algorithm (illustrated in Figure 1):

1. An initial population of structures is generated randomly and their energies evaluated at the chosen level of theory (DFT in our case, see more details below).
2. The surrogate energy model is trained with these evaluated structures and their energies, and the structure population is updated.
3. New candidate structures are generated.
4. The new candidates are locally relaxed using the surrogate model.

5. The most promising candidate according to an acquisition function is evaluated explicitly by a single-point DFT calculation and added to the population.
6. The surrogate model is retrained with the updated population. Subsequent cycles start on step 3.

The quality of the putative GM structure found strongly depends on the number of cycles, up to a certain point where the algorithm converges (albeit not always to the real GM). Convergence is reached sooner for smaller systems, and we therefore allow a different number of cycles for structures of different size:

- 200 cycles for stoichiometries of free-standing Pt_3O_x.
- 300 cycles for stoichiometries of free-standing Pt_6O_x.
- 400 cycles for stoichiometries of supported Pt_3O_x.
- 800 cycles for stoichiometries of supported Pt_6O_x.

For the generation of new candidates, the GOFEE method uses three different approaches. For the initial population it generates the candidates by placing the atoms randomly inside a box, checking that the atoms are not too close or too far from each other. For subsequent additions of candidates, two other strategies are also used, Permutation and Rattling, both transforming pre-existing structures. Permutation exchanges the positions of two atoms of different elements selected at random and Rattling displaces one or more atoms in a structure by a random distance. The approach used to create a new candidate is chosen stochastically among these three. The probabilities of selecting each approach are provided as a parameter, which in the present work have been established as 0.6, 0.2, and 0.2 for random placement in a box, permutation and rattle mutation generators, respectively. For the fully reduced systems, in which position of no O atom is globally optimized, Pt and O atoms cannot be permuted and we chose 0.8 and 0.2 probabilities of random placement in a box and rattle mutation, respectively.

One must note that convergence to the global minimum is not ensured by any single run of the GOFEE algorithm[40] (or in general of any other global optimization method[31]). To minimize the probability of missing the global minimum, we carry out at least two GOFEE runs for each stoichiometry. If the two runs converge to the same structure we do not execute additional runs. If the two runs do not converge to the same structure, we

execute additional runs until the same putative global minimum is obtained twice. As a disclaimer, we emphasize that despite the quality of the structure found following this optimization strategy, one still cannot be absolutely certain of having found the true global minimum. Due to the need to evaluate the energy of a large number of structures during the automated search for a global minimum, the DFT calculations during the GOFEE runs have been carried out using low-precision settings and a simplified model of the CeO_2(111) surface. The best structures for each stoichiometry have been subsequently recalculated at increasingly computationally demanding (and more precise) levels of theory (see next subsection for more details).

Our approach to optimize the structure of PtO_x particles uses five different levels of theory (i.e. combinations of parameters, exchange-correlation functionals, corrections, and structural models). The single-point calculations executed during each GOFEE run are carried out using low-level settings (as detailed below). All evaluated structures are subsequently filtered and relaxed at increasing levels of theory using low-level, mid-level and high-level local relaxations. These levels are briefly summarized in Figure 2 and described in more detail in the following sections. Before each set of local relaxations at a higher level of theory, structures are filtered to avoid duplicates by using the bag-of-bonds method.[31] This sorts the interatomic distances of a particle by length, and compares this list of distances between particles. Two particles are considered equal if δ_{max} and d_{max}, as defined in Ref. [31], are smaller than 0.3 and 0.7, respectively. Non-duplicate structures > 5 eV less stable than the obtained putative GM are also discarded. Due to the large number of structures and the limits of the bag-of-bonds approach when dealing with supported structures, in CeO_2-supported systems, an additional human-guided selection method is employed, where similar structures that have not been discarded by the bag-of-bonds method are excluded from subsequent relaxations. This approach allows saving considerable computational resources by filtering out unfit or duplicated structures at each level, only performing the increasingly costly optimizations on more promising structures.

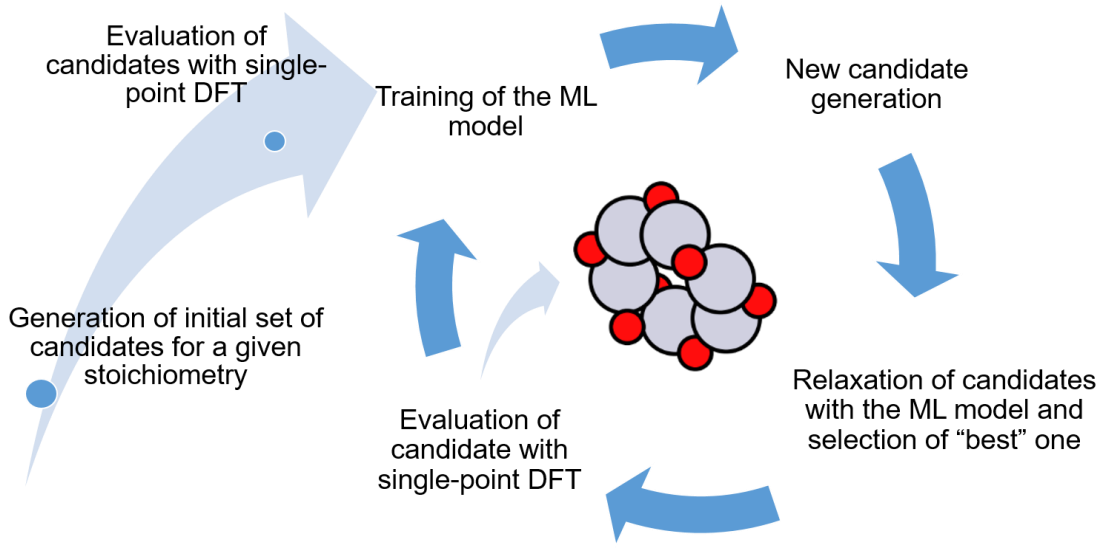

Figure 1: Schematic representation of the GOFEE algorithm using machine learning (ML) surrogate models trained on-the-fly with single-point density functional theory (DFT) calculations.

2.2. Density functional theory calculations

The electronic structures of the considered systems have been determined by means of periodic calculations based on DFT. To this end, the Vienna Ab Initio Package (VASP)[43,44] has been employed. Free-standing particles were placed in a cubic cell of size 12 Å × 12 Å × 12 Å, which ensures negligible interactions between particles in neighbouring cells while keeping calculations computationally affordable. For ceria-supported particles the oxide surface is represented by a 4×4 supercell of the CeO_2(111) surface, with 12 Å of vacuum layer above the oxide slab. For all calculations the Brillouin zone is sampled using only the Γ point. In order to account for the interaction between the frozen core electrons and the valence electrons described explicitly by the electronic wave function, VASP uses the projector augmented wave method of Blöchl.[45] All of the levels of theory share the aforementioned common characteristics of cell size and reciprocal space sampling. The low-, mid- and high- levels of theory use the Perdew-Wang (PW91) exchange-correlation functional[46] offering a good compromise between accuracy and computational cost. Low-level settings employ a single O-Ce-O tri-layer slab to represent the ceria surface, which is kept fixed with its atoms at the corresponding bulk positions. Spin-polarization is not allowed at this level, and the energy difference thresholds controlling the convergence of the self-consistent field are set to 10^{-4} eV, the

plane wave basis set energy cut-off is set for the minimum value defined by the PAW potentials for each atomic species (300 eV), and the PREC=Low flag of VASP is used. The local optimization of selected structures at the low-level settings only relaxes the Pt_yO_x particle, keeping all atoms of the ceria surface fixed, with a quite loose force convergence criterion of 0.1 eV/Å for the ionic relaxation.

The mid-level introduces the Hubbard +U correction. (i.e. DFT+U, with U= 4 eV), where a Coulomb-like interaction is applied only to the Ce4f valence orbitals, leading to the PW91+4 approach.[2,7,47] This partially corrects the inherent self-interaction error of semi-local density functionals, which otherwise insufficiently localize strongly correlated d and f electrons. The mid-level of theory also adds a second CeO_2 tri-layer to the surface slab model. The geometry of the upper CeO_2 tri-layer in contact with the Pt_yO_x particle is also allowed to relax, while the bottom tri-layer remains fixed. The converge parameters are the same as in the low-level relaxation.

The high-level approach adds spin polarization, increases the energy cut-off of the plane wave basis set (to 400.0 eV) and increases the precision of the calculations setting the PREC=High in VASP. Force convergence criterion is reduced to 0.05 eV/Å for the ionic relaxation. Although more computationally expensive, these calculations are performed over a small number of already optimized structures, and serve the purpose of obtaining accurate properties of the best surviving candidates.

A final relaxation of the most promising candidates has been performed using the HSE06 hybrid functional,[48–50] which includes a fraction of the exact Hartee-Fock exchange to overcome limitations of semi-local approximations to the exchange-correlation functional (instead of the Hubbard (+U) correction, which is no longer used). For the $Pt_3O_x/CeO_2(111)$ models, all structures relaxed at the high level have been re-relaxed with the HSE06 functional, whereas for the $Pt_6O_x/CeO_2(111)$ models we relaxed only the putative GM structure resulting from single-point evaluations with the HSE06 potential on the structures obtained from the high level relaxations.

Free-standing particles are optimized directly employing the high-level criteria, as the absence of a slab involves a drastically reduced computational cost and the final HSE06 relaxation is performed on all high-level optimized structures. In order to compare the difference between single-point evaluations using the HSE06 functional on structures optimized at the PW91+4 level and structural relaxations directly at the HSE06 functional, we have ensured that self-consistent field is converged for the 1st step of the

structural relaxation with the HSE06 functional.

We note that the transfer of electrons from the fully reduced Pt particles to the Ce^{4+} centres of the underlying oxide support is expected to slightly lower the energy of ceria-supported Pt_3 and Pt_6 systems, less than ~0.3 eV, as found for Pt_8 particles supported on $CeO_2(111)$ using the PW91+4 approach.[51] Since the low- and medium-level relaxations are carried out without spin polarization, no states with electrons occupying Ce4f orbitals are found. However, we expect such small energy differences to have a small effect on the resulting phase diagrams, particularly in the relevant regimes corresponding to $\Delta\mu_O >$ -2.0 eV (*vide infra*).

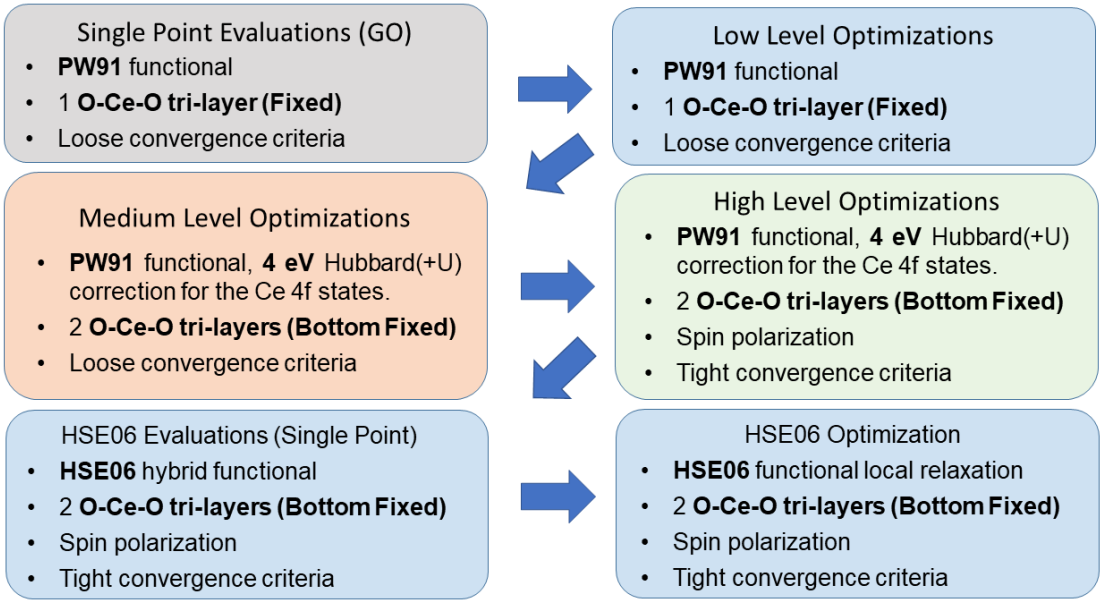

Figure 1. Schematic representation of the different levels of theory employed for the evaluation of the energy of the considered structures. The global optimization (GO) with the GOFEE code is carried out for every stoichiometry using the PW91 functional, 1 O-Ce-O tri-layer for representing the $CeO_2(111)$ surface, and using loose convergence criteria. The most stable structures are recalculated at subsequently more precise and computationally demanding levels of theory.

2.3. Ab Initio thermodynamics

Having obtained the putative GM for all considered stoichiometries, it is necessary to assess which stoichiometry is most stable under different environmental conditions.

Taking the formation energies using only the as-calculated absolute DFT energies is insufficient, since the stability of each oxidation state depends on how easy or hard it is to obtain O atoms from the gas-phase environment in contact with these particles. We therefore carry out an *ab initio* thermodynamics (AITD) analysis, which allows obtaining Gibbs free energies of formation as a function of macroscopic properties of the system from energies obtained by *ab initio* methods at 0 K.

We calculate the Gibbs free energies of each state within the canonical ensemble. This assumes constant volume, temperature, and number of atoms of the system. We further assume the Pt_yO_x particles to be in equilibrium with a gas-phase reservoir of O_2, which allows us to express the Gibbs free energy (G) of the system as a function of temperature (T) and oxygen pressure (p_{O2}). For any structure, the Gibbs free energy is calculated according to equation 1:

$$G\left(\mathrm{Pt_yO_x/CeO_2}\right) = U + TS + pV = U\left(\mathrm{Pt_yO_x/CeO_2}\right) + F^{\mathrm{vib}} + F^{\mathrm{conf}} + pV \quad (1),$$

where the internal energy (U) can be approximated as the total energy obtained in the DFT calculations of the system. F^{vib} and F^{conf} correspond to the vibrational and configurational contributions to the free energies, respectively. The Gibbs free energy of formation for the platinum oxide clusters is, thus, the difference of the Gibbs free energy of the oxide cluster with the Gibbs free energy of the fully reduced cluster and the chemical potential of oxygen, related to temperature and pressure, see equation 2.

$$\Delta G_f\left(\mathrm{Pt_yO_x/CeO_2}\right) = G\left(\mathrm{Pt_yO_x/CeO_2}\right) - G\left(\mathrm{Pt_y/CeO_2}\right) - x\mu_{\mathrm{O}}(T,P) \quad (2)$$

For the solid phase systems, the ΔF^{conf} and $\Delta(pV)$ terms are not significant at the pressures and temperatures typical of operando catalytic processes.[41,52] The F^{conf} and pV terms are similar for the different stoichiometries and basically cancel out when calculating relative (e.g. formation) free energies. In turn, the vibrational contribution F^{vib} of small and supported ZnO_x clusters were evaluated in previous work[35] and found to depend on the low frequency contributions of the metal atoms only. The difference between clusters with the same number of metal atoms is therefore small. The differences in zero-point energy (ZPE) contributions were found to be more significant, but proportional to the number of O atoms. Based on these results, we approximate the differences in ZPE by adding 0.09 eV per O atom in the particle.[35]

The chemical potential of oxygen in the gas phase is evaluated in terms of the temperature and partial pressure of the molecular oxygen reservoir and the ZPE-corrected DFT energy of molecular oxygen. Hence, for any temperature and oxygen partial pressure values the chemical potential can be expressed as shown in equation 3:

$$\mu_O = \frac{E^{DFT}{}_{O_2} + \Delta\mu_{O_2}(T, p_{O_2})}{2} = \frac{E^{DFT}{}_{O_2}}{2} + \Delta\mu_O(T, p_{O_2}) \quad (3)$$

With these approximations, the Gibbs free energy of formation for any Pt_yO_x, particle in any given chemical potential of oxygen is obtained as:

$$\Delta G_f(Pt_yO_x/CeO_2) = E^{DFT}(Pt_yO_x/CeO_2) - E^{DFT}(Pt_y/CeO_2) - x\left(\frac{E^{DFT}{}_{O_2} + E^{ZPE}{}_{O_2}}{2} + \Delta\mu_O(T, p_{O_2})\right) \quad (4)$$

For the free-standing particles, the same approximations are used, substituting the DFT energy of the ceria supported reduced particle by that of the free-standing particle. We use the same assumptions and approximations about the ΔF^{conf}, ΔF^{vib}, and $\Delta(pV)$ terms as for the ceria-supported particles, although these might not hold so well. Nonetheless, a complete vibrational analysis of the free-standing particles falls out of the scope of the present work. A useful analysis tool obtained from this treatment are the phase diagrams where the most stable phase at different chemical potentials corresponds to the state with the lowest ΔG_f.

3. Results and discussion

3.1. Structure, growth, and oxidation of the Pt_yO_x particles

We begin by describing the minimum energy structures found during the global minimum search employing the GOFEE method. The considered Pt_yO_x stoichiometries are y=3 or 6 and x=0 - 2y, both free-standing and supported on a CeO_2(111) surface, which amounts to 40 systems differing in composition.

For each system a large number of structures were evaluated with DFT (up to 1613 for a single run of the most complex system – ceria supported Pt_6O_{12}) in order to locate the GM. After subsequent relaxations at increasing levels of theory, ~10 structures per

stoichiometry are recalculated at the final HSE06 level for the $Pt_3O_x/CeO_2(111)$ system and only the putative GM for the $Pt_6O_x/CeO_2(111)$ system. For the free-standing systems, 258 structures in total are finally relaxed at the HSE06 level. We note that this optimization procedure often identifies one or several low-lying meta-stable conformers with energy differences < 0.3 eV with respect to the putative global minimum. This has no effect in the as-formulated phase diagrams, but can lead to effects on the ensemble properties of these systems, similarly to what was reported for supported metal and oxide clusters by Alexandrova and co-workers.[53–55]

The global minima obtained for the unsupported particles are depicted in Figure 3. For the fully or highly reduced structures, triangular Pt_3 motifs are prevalent and the structures are quite planar. As the particle becomes oxidized, it loses flatness to accommodate the oxygen atoms while maintaining some symmetry (e.g. a mirror plane). This is characteristic for Pt_6O_x stoichiometries in low oxidation states. Higher oxidation states, on the other hand, become either ringed or clustered, adopting one conformation or the other based on the oxygen-to-platinum ratio. Certain O:Pt ratios favor one structure or the other based on the possibility of adopting stabilizing structural features.

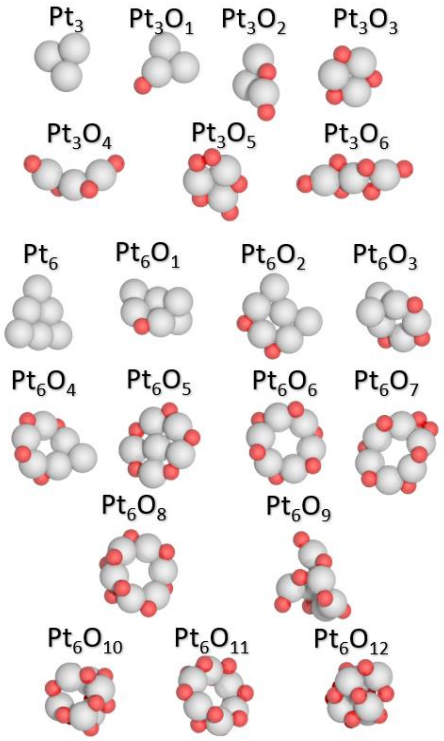

Figure 3. Most stable structures found for each stoichiometry of the free-standing Pt_3O_x and Pt_6O_x particles. Red and grey spheres correspond to O and Pt atoms, respectively.

Oxygen atoms preferentially bridge two Pt atoms. Additionally, some stoichiometries have global minima with oxygen atoms placed in terminal positions. PtO_x structures are therefore characterized by Pt-O-Pt angles between 80º and 100º, quasi-linear O-Pt-O fragments, and Pt-O bond distances ~1.9 Å. Once every bridge position between platinum pairs is filled, O atoms start to doubly occupy (opposite) bridge positions between two same Pt atoms, giving rise to the formation of planar PtO_4 motifs for highly oxidized states. Quasi-molecular forms of O pairs also appear in stable structures (see e.g. Pt_6O_7), although such motifs appear less frequently and structures containing them are generally not thermodynamically stable compared to other stoichiometries. The same structural motifs are typical for the ceria-supported global minima (see Figure 4). However, the presence of the cerium oxide surface impedes the formation of strictly planar structures. Platinum atoms bind to oxygen atoms of the ceria surface and the oxygen atoms of the particle tend to locate near Ce. Since distances between oxygen atoms in the ceria surface (~3.8 Å) are larger than the Pt-Pt bond distances (2.4 Å fully reduced, ~2.6 Å O bridged), there is a size mismatch that causes the smaller particles to adopt triangular conformations where only two platinum atoms are in contact with the surface.

For the Pt_3O_1-$CeO_2(111)$ and Pt_3O_5-$CeO_2(111)$ structures, a new motif appears where an oxygen atom is located between three platinum atoms. This is favorable because it forms three linear O-Pt-O motifs with the oxygen positions in the surface, which confers enough stability to the particle to compensate the differences between the Pt-Pt bond length and the distance between surface oxygen atoms. The mismatch between the surface O-O distance and Pt-Pt bond length is less notable for the Pt_6O_x stoichiometries due to the increased degrees of freedom, which allow the particle to adapt better to the surface. However, the tendency to form linear O-Pt-O bonds still proves to be significant since the observed minima include these motifs in all their structures, often using ceria lattice O atoms to construct these linear motifs.

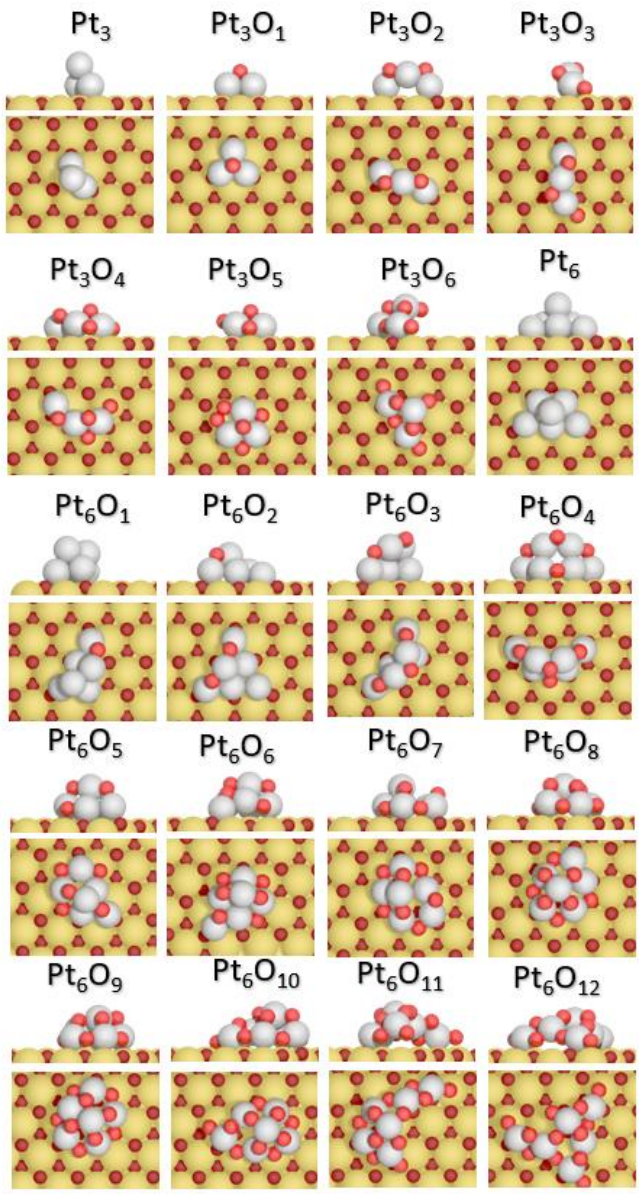

Figure 4. Most stable structures found for each stoichiometry of the Pt_3O_x and Pt_6O_x particles supported on CeO_2 (111). Ce atoms are beige and lattice O atoms are dark red. Other atoms are coloured as in Figure 3.

For low and medium oxidation states, the particles form more compact structures (e.g., $Pt_6O_9/CeO_2(111)$) where O atoms are shared between multiple platinum atoms. However, as particles become more saturated with oxygen atoms, they tend to spread over the surface, increasing the average coordination of Pt atoms while avoiding oversaturating individual platinum atoms. Therefore, the two main differences between the conformations adopted by the $CeO_2(111)$-supported particles and the free-standing ones are due to the topology of the CeO_2 surface and to the possibility to form the

aforementioned stable motifs with the O atoms of the ceria surface.

3.2. Phase diagrams of the Pt_yO_x global minima

The free energy variation of the global minima found for each stoichiometry at different chemical potentials of the O_2 reservoir is evaluated employing AITD as described in section 2.3. The Gibbs free energy of formation (ΔG_f) at each value of the chemical potential of the molecular oxygen reservoir (μ_O) for the global minimum of each stoichiometry is determined by equation 4. This allows the construction of phase diagrams where ΔG_f for each global stoichiometry is plotted in a range of μ_O, identifying the most stable stoichiometry for each value of the chemical potential and the values of μ_O at which phase transitions occur.

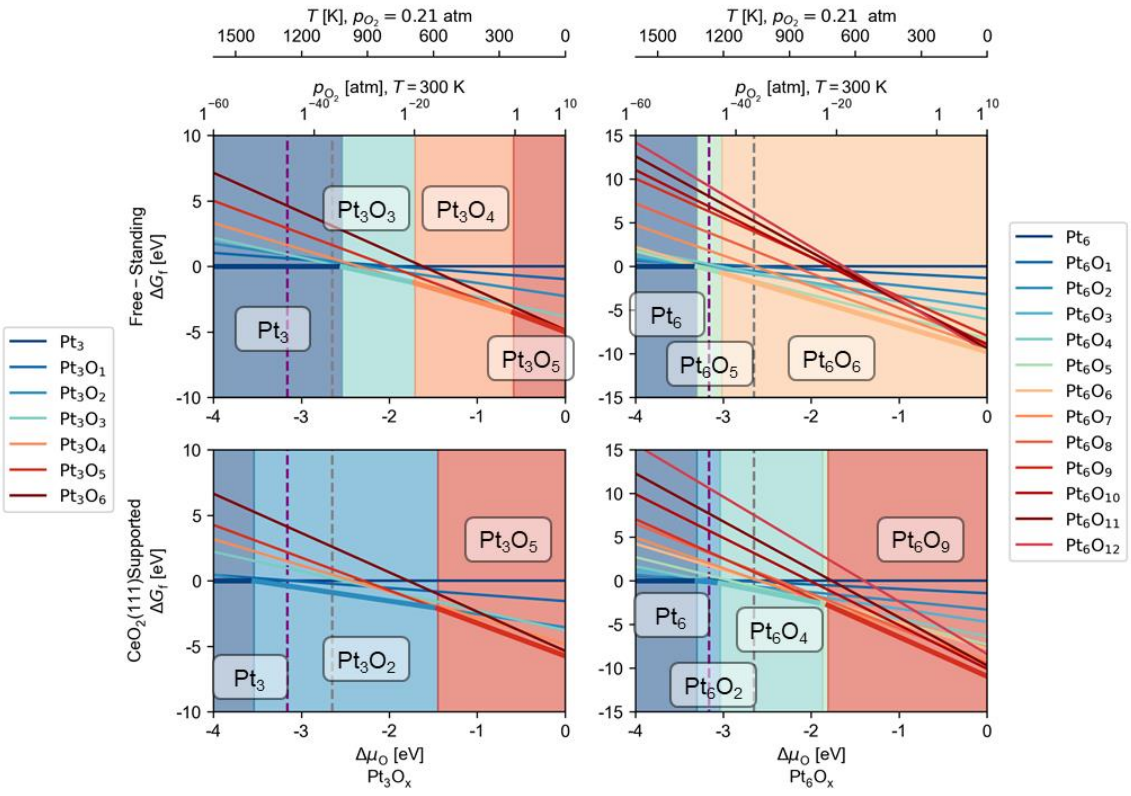

Figure 5. Phase diagrams for the free-standing (top) and $CeO_2(111)$-supported (bottom) Pt_yO_x systems calculated at the HSE06 level of theory. Each line corresponds to a different stoichiometry, and the most stable state in each region of μ_O is labelled accordingly. . Vertical dotted lines at -2.7 eV *and* -3.2 eV indicate calculated values of μ_O from the literature,[50,56] at which O vacancies would appear in the $CeO_2(111)$ surface *and* at which CeO_2 is reduced to Ce_2O_3, respectively.

The phase diagrams for the free-standing Pt_yO_x and $CeO_2(111)$-supported Pt_yO_x

particles calculated after relaxing the best candidates at the HSE06 level of theory are shown in Figure 5, indicating the more stable stoichiometry for each value of μ_O. Common to all systems, higher (less negative) values of μ_O (corresponding to more oxidizing environments) increase the stability of stoichiometries with a higher oxidation state, a direct consequence of the thermodynamic equilibrium with a molecular oxygen reservoir from which it is easier to extract O from (i.e. with a higher chemical potential to react). Notably, partially oxidized states are stable for a wide range of μ_O, including very reducing conditions of down to $\Delta\mu_O \sim -3$ eV.

For the free-standing and ceria-supported Pt_3O_x, the most stable structure at $\Delta\mu_O=0$ eV (T= 0K) is that with the Pt_3O_5 stoichiometry. For the free-standing Pt_6O_x system, Pt_6O_6 is the most stable configuration at $\Delta\mu_O=0$ eV, probably due to O:Pt ratio allowing it to form a very stable ringed structure with the stable linear O-Pt-O and angled Pt-O-Pt motifs. For the ceria-supported Pt_6O_x systems the Pt_6O_9 structure made only of planar PtO_4 motifs is the most stable under very oxidizing conditions (high $\Delta\mu_O$), indicating the stability of such structural motifs. The evolution of the systems as $\Delta\mu_O$ decreases (e.g. temperature increases at fixed p_{O2}, as indicated in the upper x axis of Figure 5) is discussed next. Free-standing Pt_3O_5 is reduced at $\Delta\mu_O \sim -0.6$ eV to Pt_3O_4, and then to Pt_3O_0 at $\Delta\mu_O \sim -2.3$ eV. For the ceria-supported Pt_3O_x system, Pt_3O_5 is stable for a wider range of $\Delta\mu_O$ than its free-standing counterpart, becoming reduced to Pt_3O_2 at $\Delta\mu_O \sim -1.4$ eV, and later to Pt_3O_1 at $\Delta\mu_O \sim -3.8$ eV. Free-standing Pt_6O_6 is stable for a wide range of $\Delta\mu_O$ and is reduced to Pt_6O_0 only at $\Delta\mu_O \sim -3.2$ eV. Ceria-supported Pt_6O_9 is in turn reduced to Pt_6O_5 at $\Delta\mu_O \sim -1.8$ eV. In further reducing environments ($\Delta\mu_O \sim -1.8$ eV), the triangular Pt_6O_2 structure becomes the most stable, and Pt_6O_0 is reached at $\Delta\mu_O \sim -3.3$ eV.

These results demonstrate that the ceria surface contributes to stabilizing more oxidized states of the PtO_x particles for some regions of the phase diagrams, but stabilizes more O-deficient states for others. A general stabilization of more O-deficient states would be expected due to the oxidizing behavior of the ceria surface, but our calculated phase diagrams reveal that intricate effects related to the kind of structures and structural motifs that each stoichiometry can form are more relevant than the oxidizing capacity of ceria.

The two-dimensional phase diagrams of these systems in terms of composition as a function of p_{O2} and T values (shown in Figure 6) reveal even more clearly the wide range of conditions under which O-containing states of sub-nano Pt particles are stable.

This is in good agreement with results obtained by Wang et al. using a grand canonical Monte Carlo sampling approach,[27] where a Pt_8O_{14} cluster was identified as most stable at 350 K and p_{O2} = 0.05 atm. A recent study evaluating the oxidation states and resulting activity of ceria-supported Pt particles at low temperatures have also proposed the presence and relevance of PtO_x clusters.[25] Fully reduced Pt particles without any additional O atoms on them are in fact thermodynamically stable only at very high T and very low p_{O2} values, which suggests that studies addressing the properties of ceria-supported Pt clusters also must consider such oxidized states, and that previous understanding of such materials based on calculations using only fully reduced Pt clusters may be incomplete.

The stability of the O-rich PtO_x particles is also one of the factors favouring the migration of O atoms from ceria to Pt (i.e. the reverse spill-over mechanism) identified in previous works.[7,29] Considering the value of $\Delta\mu_O$ = -2.7 eV at which O vacancies were predicted to appear in $CeO_2(111)$[56] (see vertical dotted lines in Figure 5), it can be concluded that Pt particles would be fully reduced on $CeO_2(111)$ well after the appearance of O vacancies in the ceria surface, or that O atoms will oxidize Pt particles before healing diluted O vacancies in $CeO_{2-x}(111)$. However, we expect O vacancies to affect the structure of supported PtO_x particles. Therefore, further clarifying the interplay between the oxidation state of Pt particles and the formation of O vacancies in ceria surfaces would require global optimizations on reduced ceria surface models.

Accepted to J. Chem. Phys. 10.1063/5.0099927

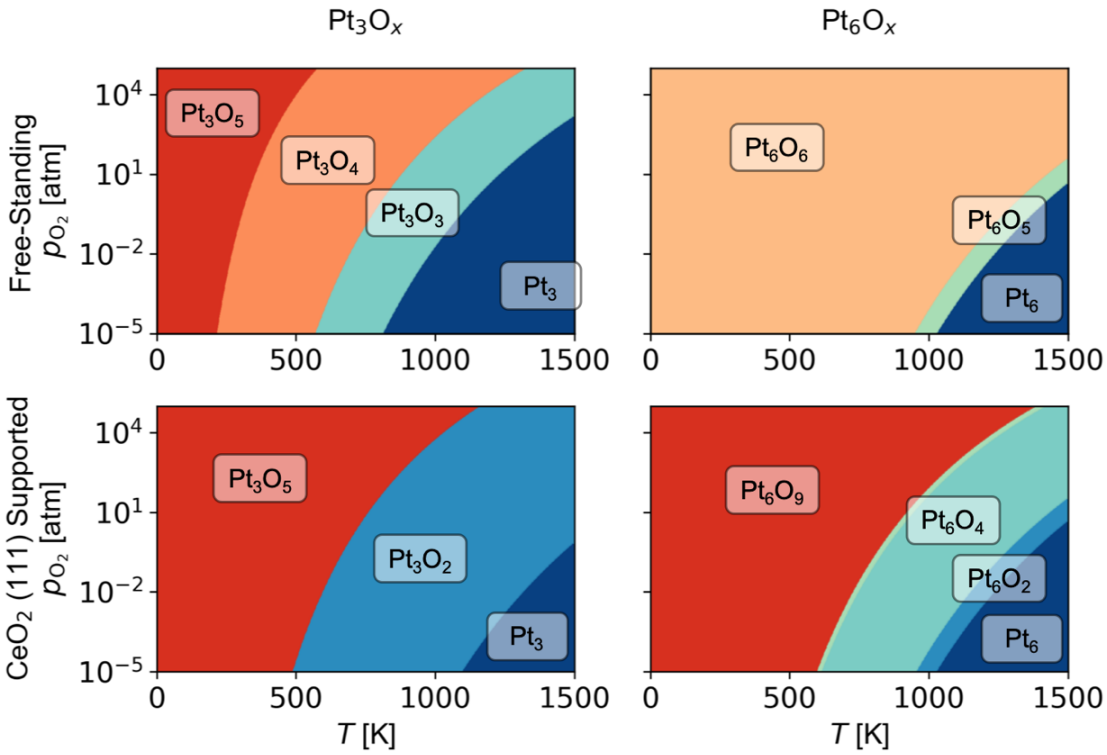

Figure 6. Phase diagrams as a function of p_{O2} and T for the free-standing (top) and CeO_2(111)-supported (bottom) Pt_3O_x and Pt_6O_x systems calculated at the HSE06 level of theory.

3.3. Effect of the exchange correlation functional on phase transitions

Having calculated the total energy of the GM structures with different approaches allows us to evaluate the differences in predicted phase stability when using different levels of theory. Semi-local exchange correlation functionals, such as PW91, are known to underestimate the binding energy of the O_2 molecule (and of O_2-like local motifs). This affects the calculated phase diagrams by spuriously stabilizing systems with higher O contents with respect to less O-rich ones, but the extent of such differences is unclear. In order to quantify it, we compare in Figure 6 the evolution of the O:Pt ratio with $\Delta\mu_O$ obtained by means of a) the aforementioned high-level approach (PW91+4 with high precision settings), b) single-point calculations with the HSE06 functional on structures optimized with the high-level approach, and c) structural relaxations with the HSE06 functional of the structures obtained using the high-level approach. The corresponding phase diagrams obtained with the PW91+4 approach and by single-point HSE06 calculations are shown in Figures S1 and S2, respectively.

For all evaluated systems, the PW91 functional generally leads to either equal or larger O:Pt ratios with respect to the HSE06 results depending on the $\Delta\mu_O$ range. This indicates that the high-level approach using the PW91 functional approximates rather well, albeit not perfectly, the phase stabilities predicted using the HSE06 functional. Importantly, O-rich states are prevalent for a wide range of conditions for both functionals, which suggests that similar conclusions are reached and that the computationally demanding HSE06 functional is not necessary for obtaining reasonably accurate phase diagrams for PtO_x sub-nanometer particles. Furthermore, differences in predicted phase stability are even smaller between HSE06 single-point evaluations of the energy of structures optimized at the PW91+4 level and those obtained relaxing structures with HSE06. This suggests that when using the HSE06 functional, single-point calculations on structures optimized with semi-local exchange-correlation functionals already provide an accurate representation. One can therefore produce sufficiently precise phase diagrams without the need to perform the costly structural relaxations at the HSE06 level.

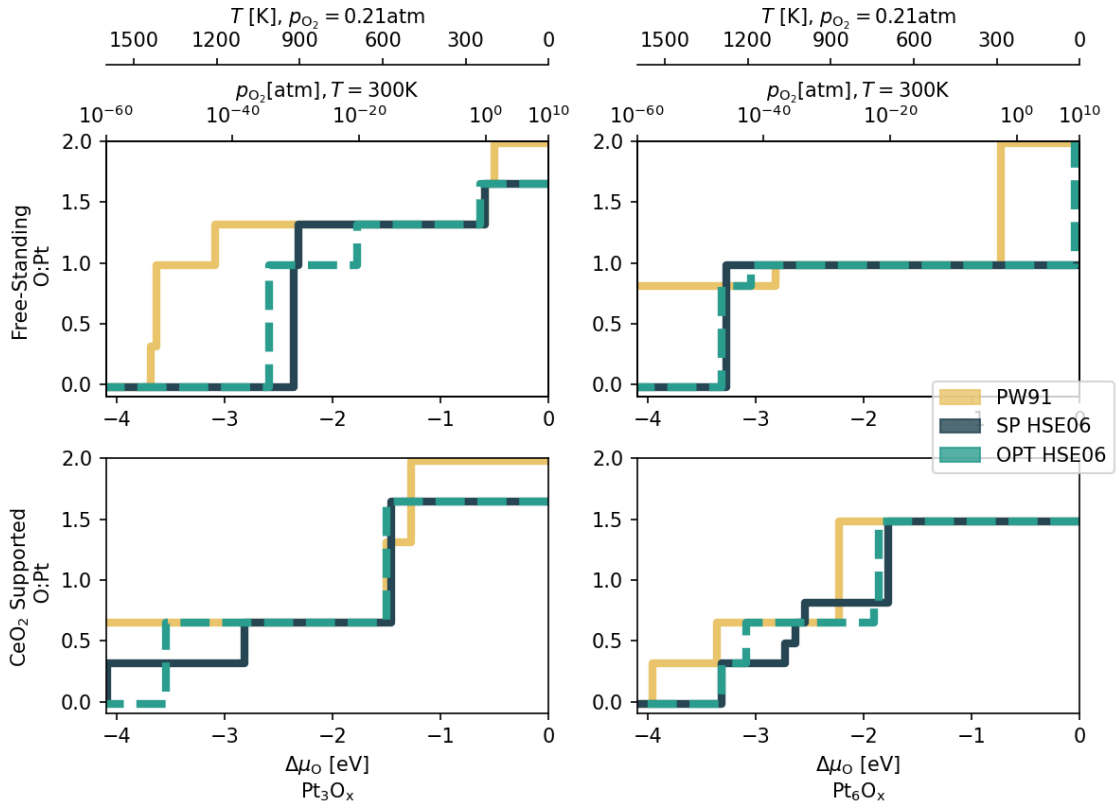

Figure 7. Evolution of the O:Pt ratio as a function of $\Delta\mu_O$ for the free-standing (top) and CeO_2(111)-supported (bottom) Pt_yO_x clusters. PW91, SP HSE06, and OPT HSE06 correspond to values obtained locally relaxing with the PW91+4 functional, with single-point calculations with

HSE06 on structures relaxed with the PW91+4 functional, and locally relaxing with the HSE06 functional, respectively.

3.4. Atomic charges of global minima structures

We now address the evolution of charges of Pt atoms upon oxidation of the studied systems. The atomic Pt charges of the most stable oxidation states of each system (calculated using Bader's atoms in molecules approach)[57] are shown on Figure 8.

All systems under scrutiny follow similar trends in their charge distribution and evolution with the number of O atoms. Not unexpectedly, as the system increases its oxidation state, so does the average charge of its Pt atoms. The charges of individual Pt atoms also follow a similar trend – Pt atoms become more positively chargesd when bonded to a larger number of O atoms. For platinum atoms coordinated to a single oxygen atom, the charge is approximately 0.0-0.2 |e|. For Pt atoms bonded to two oxygen atoms, the charge increases to 0.6-1.0 |e|, while higher coordination numbers (i.e. Pt atoms in PtO_4 motifs) exhibit charges between 1.0-1.5 |e|. In addition, O atoms that are bonded only to one Pt atoms have a stronger oxidizing effect than those bonded to two Pt atoms (see e.g. free-standing Pt_3O_4).

The dependence of the atomic Pt charge on the local coordination leads to inhomogeneous charge distributions in particles that do not have enough O atoms for adopting a structure where all Pt atoms have a similar coordination. This seems to have strong implications for the system stability, since highly stable structures that dominate the phase diagrams (such as free-standing Pt_6O_6 and ceria-supported Pt_6O_9) are characterized by a quite homogeneous charge distribution. It is also notable that the oxidizing effect of O atoms of the ceria surface on the charge of the platinum atoms is lower than that of the O atoms adsorbed directly on the Pt cluster. For example, the Pt atoms of the Pt_3O_5 particle appear to be more oxidized for the free-standing case than for the ceria-supported structure, despite the contact to atoms from the ceria surface. Thus, although the $CeO_2(111)$ surface has an oxidizing effect on the particles and allows to complete certain stable structural motifs, bonds formed with O atoms from the ceria lattice are significantly less oxidizing than those with O atoms directly on the PtO_x particles.

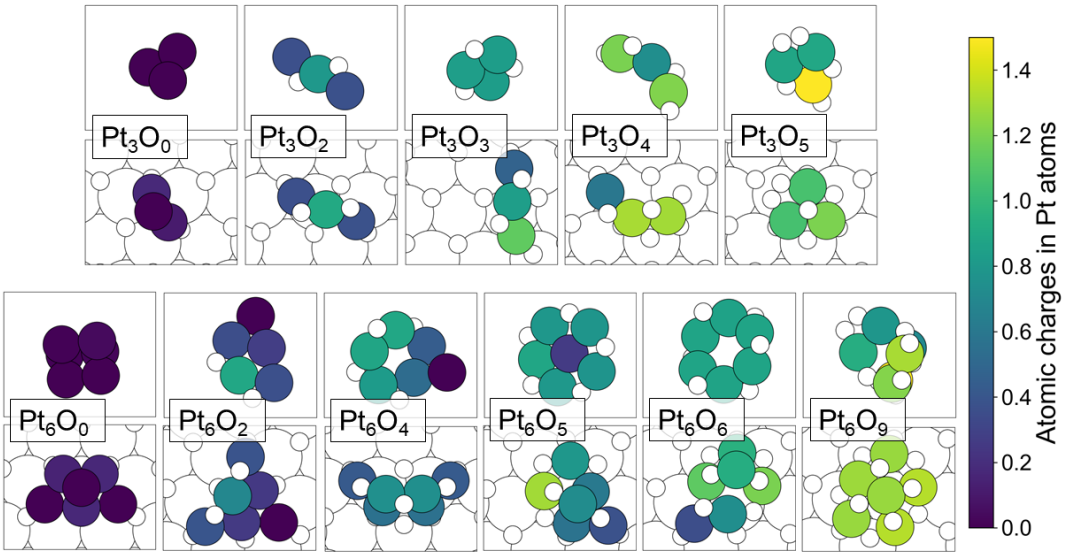

Figure 8. Charge distribution for the Pt atoms on each of the most stable oxidation states of the considered systems. Pt atoms are coloured according to their Bader charge in |**e**|. For clarity, O and Ce atoms are represented as small and large white circles, respectively.

4. Conclusions

In this work, a systematic global optimization scheme has been adapted and employed to characterize free-standing and $CeO_2(111)$-supported Pt_yO_x structures, with y=3 and 6 and x=0-2y. The global optimization for each stoichiometry has been carried out with the GOFEE method, a novel approach which has proven to be fast and computationally efficient.

The morphological analysis of the obtained putative global minima has revealed several structural motifs that are present in stable structures. Namely, the linear O-Pt-O, angled Pt-O-P (80-100º), square-planar PtO_4 formations, and quasi-molecular O pairs. The $CeO_2(111)$ surface participates in the formation of such motifs, which leads to rather spread out structures for highly oxidized states. The *ab initio* thermodynamics analysis of the obtained global minima has revealed that oxidized particles are stable over a rather wide range of oxygen chemical potentials μ_O. Although the $CeO_2(111)$ surface has a slightly oxidizing effect, it does not stabilize PtO_x particles with fewer O atoms for all values of μ_O. This is related to the fact that O atoms of the $CeO_2(111)$ have a much weaker oxidizing ability than O atoms directly in the PtO_x clusters, as revealed by a detailed charge analysis. The stability of certain stoichiometries for supported and free-standing

PtO_x particles are instead related to the possibility of forming a large amount of particularly stable structural motifs.

In summary, the presented approach and resulting analysis constitute a well-grounded and computationally efficient strategy for constructing dedicated structural models of the free-standing and CeO_2(111) supported PtO_x clusters. This provides an improvement over non-machine-learning assisted global optimization algorithms or still prevalent human-guided approaches. It helps to cement the combination of *ab initio* thermodynamics with global optimization methods as a necessary step to determine the structure and oxidation states of active sites preceding DFT-based mechanistic studies in catalysis. The results of this work indicate that studies rationalizing activity of ceria-supported Pt clusters must consider oxidized states, and that previous understanding of such materials obtained only with fully reduced Pt clusters may be incomplete. Forthcoming studies comparing the chemical and catalytic properties of the different oxidation states will therefore be of pivotal importance. We expect these findings to be relevant also for clusters of other late transition metals on both inert and non-inert supports.

5. Supplementary Material

Electronic supplementary information (ESI) available: pdf file with Fig. S1 and S2 and a zip file with the atomic coordinates of optimized structures (in traj and xyz formats). See DOI:xx.xxxxx/xxxxxxxxxxx

6. Acknowledgements

Authors gratefully acknowledge support by the Spanish grants PGC2018-093863-B-C22 and MDM-2017-0767 as well as by the grants 2018BP00190 (for A.B.) and 2017SGR13 of the Generalitat de Catalunya. Computer resources have been provided by the Red Española de Supercomputación. This study was also supported the by European COST Action CA18234.

7. Data availability

All global minima structures presented in this article are available within the supplementary material and in the ioChem-BD[58] repository with the identifyiner DOI:

10.19061/iochem-bd-6-145.

6. References

[1] A. Crucq, A.F. Diwell, R.R. Rajaram, H.A. Shaw, and T.J. Truex, Stud. Surf. Sci. Catal. **71**, 139 (1991).

[2] A. Bruix, Y. Lykhach, I. Matolínová, A. Neitzel, T. Skála, N. Tsud, M. Vorokhta, V. Stetsovych, K. Ševčíková, J. Mysliveček, R. Fiala, M. Václavu, K.C. Prince, S. Bruyère, V. Potin, F. Illas, V. Matolín, J. Libuda, and K.M. Neyman, Angew. Chemie - Int. Ed. **53**, 10525 (2014).

[3] D.-H. Lim, W.-D. Lee, D.-H. Choi, and H.-I. Lee, Appl. Catal. B Environ. **94**, 85 (2010).

[4] Q. Fu, H. Saltsburg, and M. Flytzani-Stephanopoulos, Science **301**, 935 (2003).

[5] S. Aranifard, S.C. Ammal, and A. Heyden, J. Phys. Chem. C **116**, 9029 (2012).

[6] A. Trovarelli and P. Fornasiero, *Catalysis by Ceria and Related Materials*, 2nd edn (Imperial College Press, London, UK, 2013).

[7] G.N. Vayssilov, Y. Lykhach, A. Migani, T. Staudt, G.P. Petrova, N. Tsud, T. Skála, A. Bruix, F. Illas, K.C. Prince, V. Matolín, K.M. Neyman, and J. Libuda, Nat. Mater. **10**, 310 (2011).

[8] D.R. Mullins and K.Z. Zhang, Surf. Sci. **513**, 163 (2002).

[9] M. Flytzani-Stephanopoulos, Acc. Chem. Res. **47**, 783 (2014).

[10] M.A. Newton, Chem. Soc. Rev. **37**, 2644 (2008).

[11] K.F. Kalz, R. Kraehnert, M. Dvoyashkin, R. Dittmeyer, R. Gläser, U. Krewer, K. Reuter, and J.D. Grunwaldt, ChemCatChem **9**, 17 (2017).

[12] P.L. Hansen, J.B. Wagner, S. Helveg, J.R. Rostrup-Nielsen, B.S. Clausen, and H. Topsøe, Science (80-.). **295**, 2053 (2002).

[13] A. Bruix, J.T. Margraf, M. Andersen, and K. Reuter, Nat. Catal. **2**, 659 (2019).

[14] L. Grajciar, C.J. Heard, A.A. Bondarenko, M. V. Polynski, J. Meeprasert, E.A. Pidko, and P. Nachtigall, Chem. Soc. Rev. **47**, 8307 (2018).

[15] Y. Lykhach, S.M. Kozlov, T. Skála, A. Tovt, V. Stetsovych, N. Tsud, F. Dvořák, V. Johánek, A. Neitzel, J. Mysliveček, S. Fabris, V. Matolín, K.M. Neyman, and J. Libuda,

Nat. Mater. **15**, 284 (2016).

[16] Y. Zhou, J.M. Perket, and J. Zhou, J. Phys. Chem. C **2**, 11853 (2010).

[17] S.M.F. Shahed, A. Beniya, H. Hirata, and Y. Watanabe, J. Chem. Phys. **148**, 114702 (2018).

[18] X.I. Pereira-Hernández, A. DeLaRiva, V. Muravev, D. Kunwar, H. Xiong, B. Sudduth, M. Engelhard, L. Kovarik, E.J.M. Hensen, Y. Wang, and A.K. Datye, Nat. Commun. 2019 101 **10**, 1358 (2019).

[19] L. Nie, D. Mei, H. Xiong, B. Peng, Z. Ren, X.I.P. Hernandez, A. DeLaRiva, M. Wang, M.H. Engelhard, L. Kovarik, A.K. Datye, and Y. Wang, Science (80-.). **358**, 1419 (2017).

[20] F. Dvořák, M. Farnesi Camellone, A. Tovt, N.-D. Tran, F.R. Negreiros, M. Vorokhta, T. Skála, I. Matolínová, J. Mysliveček, V. Matolín, and S. Fabris, Nat. Commun. **7**, 10801 (2016).

[21] W. Tang, Z. Hu, M. Wang, G.D. Stucky, H. Metiu, and E.W. McFarland, J. Catal. **273**, 125 (2010).

[22] P. Bera, K.R. Priolkar, A. Gayen, P.R. Sarode, M.S. Hegde, S. Emura, R. Kumashiro, V. Jayaram, and G.N. Subbanna, Chem. Mater. **15**, 2049 (2003).

[23] H. Guo, H. Gao, W. Hofer, F. Rosei, I. Matolínová, R. Fiala, I. Khalakhan, M. Vorokhta, Z. Sofer, H. Yoshikawa, K. Kobayashi, and V. Matolín, Appl. Surf. Sci. **258**, 2161 (2012).

[24] J. Jones, H. Xiong, A.T. DeLaRiva, E.J. Peterson, H. Pham, S.R. Challa, G. Qi, S. Oh, M.H. Wiebenga, X.I.P. Hernández, Y. Wang, and A.K. Datye, Science **353**, 150 (2016).

[25] A.I. Boronin, E.M. Slavinskaya, A. Figueroba, A.I. Stadnichenko, T.Y. Kardash, O.A. Stonkus, E.A. Fedorova, V. V. Muravev, V.A. Svetlichnyi, A. Bruix, and K.M. Neyman, Appl. Catal. B Environ. **286**, 119931 (2021).

[26] S.M.F. Shahed, A. Beniya, H. Hirata, and Y. Watanabe, J. Vac. Sci. Technol. A **40**, 013204 (2022).

[27] H. Wang, J.-X. Liu, L.F. Allard, S. Lee, J. Liu, H. Li, J. Wang, J. Wang, S.H. Oh, W. Li, M. Flytzani-Stephanopoulos, M. Shen, B.R. Goldsmith, and M. Yang, Nat. Commun. **10**, 3808 (2019).

[28] J. Ke, W. Zhu, Y. Jiang, R. Si, Y.J. Wang, S.C. Li, C. Jin, H. Liu, W.G. Song, C.H.

Yan, and Y.W. Zhang, ACS Catal. **5**, 5164 (2015).

[29] F.R. Negreiros and S. Fabris, J. Phys. Chem. C **118**, 21014 (2014).

[30] S.C. Ammal and A. Heyden, ACS Catal. **7**, 301 (2017).

[31] L.B. Vilhelmsen and B. Hammer, J. Chem. Phys. **141**, 044711 (2014).

[32] J.X. Liu, Y. Su, I.A.W. Filot, and E.J.M. Hensen, J. Am. Chem. Soc. **140**, 4580 (2018).

[33] H. Zhai and A.N. Alexandrova, ACS Catal. **7**, 1905 (2017).

[34] B. Zandkarimi and A.N. Alexandrova, J. Phys. Chem. Lett. **10**, 460 (2019).

[35] T. Reichenbach, M. Walter, M. Moseler, B. Hammer, and A. Bruix, J. Phys. Chem. C **123**, 30903 (2019).

[36] L.B. Vilhelmsen and B. Hammer, ACS Catal. **4**, 1626 (2014).

[37] L.B. Vilhelmsen and B. Hammer, Phys. Rev. Lett. **108**, 126101 (2012).

[38] S. Bhattacharya, S. V Levchenko, L.M. Ghiringhelli, and M. Scheffler, Phys. Rev. Lett. **111**, 135501 (2013).

[39] S. Bhattacharya, S. V. Levchenko, L.M. Ghiringhelli, and M. Scheffler, New J. Phys. **16**, (2014).

[40] M.K. Bisbo and B. Hammer, Phys. Rev. Lett. **124**, 86102 (2020).

[41] J. Rogal and K. Reuter, Exp. Model. Simul. Gas- Surf. Interact. React. Flows Hypersonic Flights 2 (2006).

[42] K. Reuter, Catal. Letters **146**, 541 (2016).

[43] G. Kresse and J. Furthmuller, Phys. Rev. B **54**, 11169 (1996).

[44] G. Kresse and J. Hafner, Phys. Rev. B **47**, 558 (1993).

[45] P.E. Blöchl, Phys. Rev. B **50**, 17953 (1994).

[46] J.P. Perdew, C. J.A., V. S.H., K.A. Jackson, M.R. Pederson, D.J. Singh, and C. Fiolhais, Phys. Rev. B **46**, 6671 (1992).

[47] A. Bruix and K.M. Neyman, Catal. Letters **146**, 2053 (2016).

[48] J. Heyd, G.E. Scuseria, and M. Ernzerhof, J. Chem. Phys. **118**, 8207 (2003).

[49] J. Paier, M. Marsman, K. Hummer, G. Kresse, I.C. Gerber, and J.G. Angyán, J. Chem. Phys. **124**, 154709 (2006).

[50] M.V. Ganduglia-Pirovano, J.L.F. Da Silva, and J. Sauer, Phys. Rev. Lett. **102**, 026101 (2009).

[51] A. Bruix, A. Migani, G.N. Vayssilov, K.M. Neyman, J. Libuda, and F. Illas, Phys. Chem. Chem. Phys. **13**, 11384 (2011).

[52] K. Reuter and M. Scheffler, Phys. Rev. Lett. **90**, 046103 (2003).

[53] B. Zandkarimi and A.N. Alexandrova, Wiley Interdiscip. Rev. Comput. Mol. Sci. e1420 (2019).

[54] E.T. Baxter, M.A. Ha, A.C. Cass, A.N. Alexandrova, and S.L. Anderson, ACS Catal. **7**, 3322 (2017).

[55] G. Sun, A.N. Alexandrova, and P. Sautet, ACS Catal. 5309 (2020).

[56] J. Da Silva, M. Ganduglia-Pirovano, J. Sauer, V. Bayer, and G. Kresse, Phys. Rev. B **75**, 045121 (2007).

[57] R. Bader, *Atoms in Molecules: A Quantum Theory* (Oxford University Press, 1994).

[58] M. Álvarez-Moreno, C. De Graaf, N. López, F. Maseras, J.M. Poblet, and C. Bo, J. Chem. Inf. Model. **55**, 95 (2015).

Accepted to J. Chem. Phys. 10.1063/5.0099927

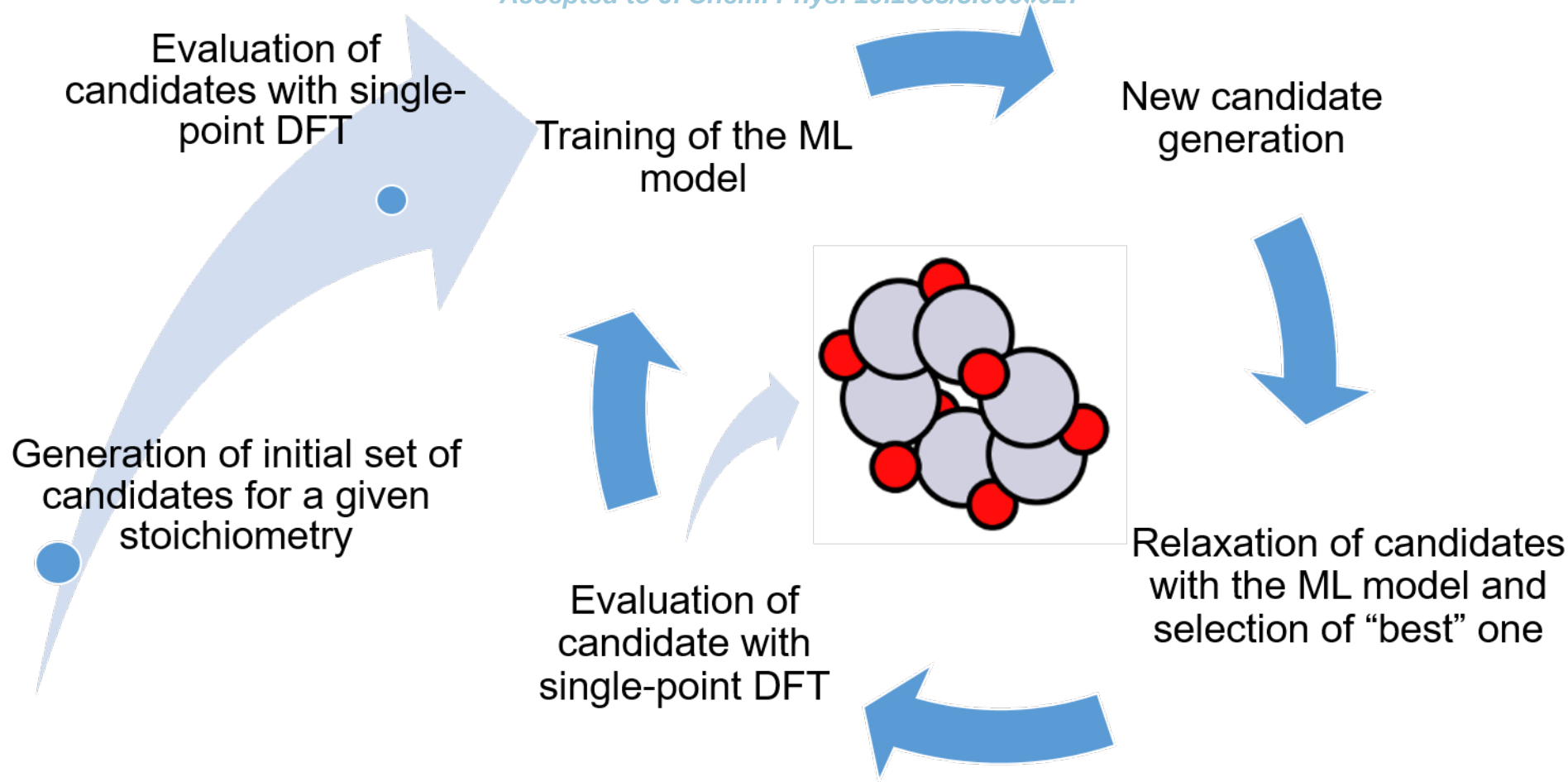

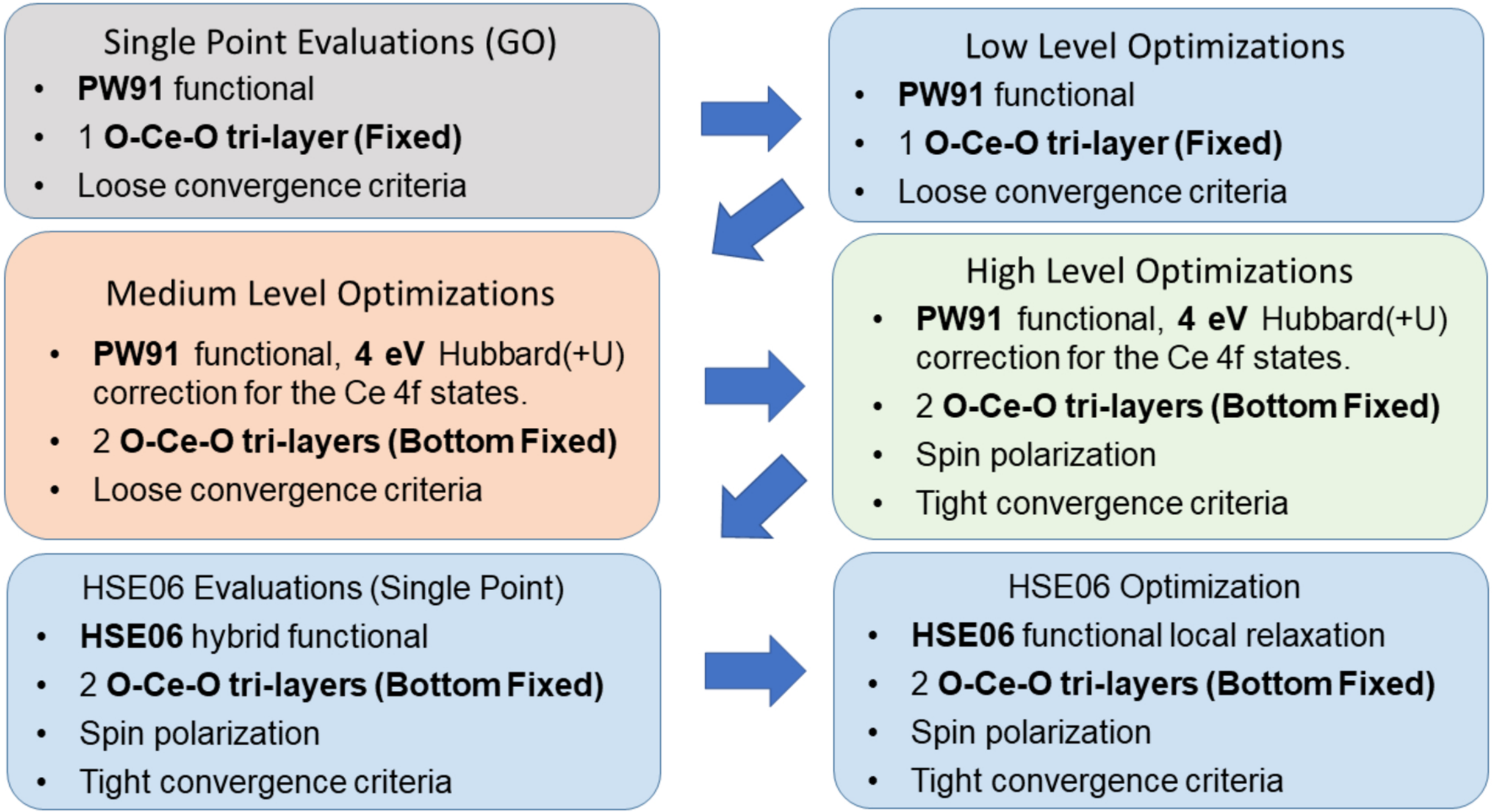
Single Point Evaluations (GO)
• PW91 functional
• 1 O-Ce-O tri-layer (Fixed)
• Loose convergence criteria
Low Level Optimizations
• PW91 functional
• 1 O-Ce-O tri-layer (Fixed)
• Loose convergence criteria
Medium Level Optimizations
• PW91 functional, 4 eV Hubbard(+U) correction for the Ce 4f states.
• 2 O-Ce-O tri-layers (Bottom Fixed)
• Loose convergence criteria
High Level Optimizations
• PW91 functional, 4 eV Hubbard(+U) correction for the Ce 4f states.
• 2 O-Ce-O tri-layers (Bottom Fixed)
• Spin polarization
• Tight convergence criteria
HSE06 Evaluations (Single Point)
• HSE06 hybrid functional
• 2 O-Ce-O tri-layers (Bottom Fixed)
• Spin polarization
• Tight convergence criteria
HSE06 Optimization
• HSE06 functional local relaxation
• 2 O-Ce-O tri-layers (Bottom Fixed)
• Spin polarization
• Tight convergence criteria

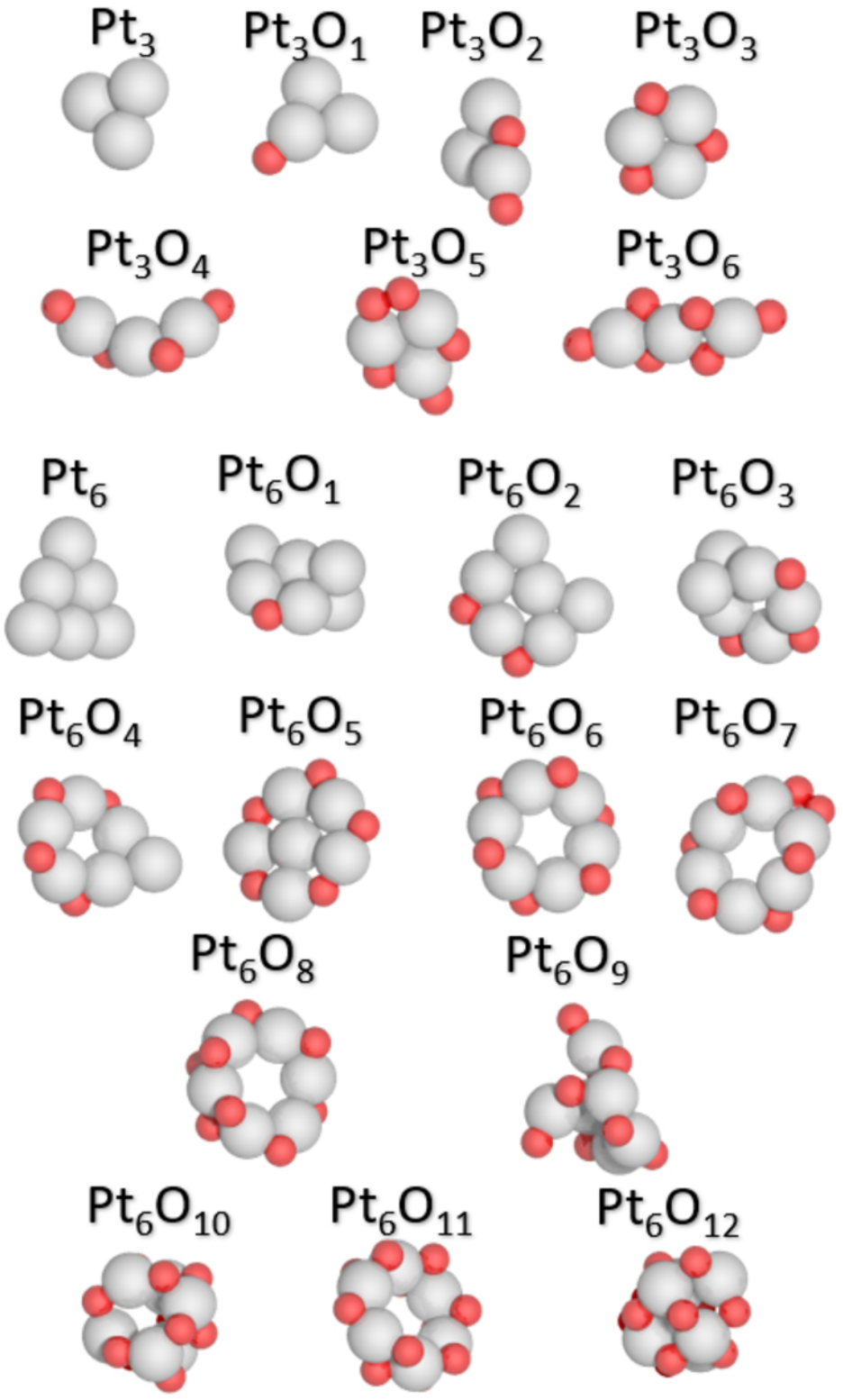
Pt_3
Pt_3O_1
Pt_3O_2
Pt_3O_3
Pt_3O_4
Pt_3O_5
Pt_3O_6
Pt_6
Pt_6O_1
Pt_6O_2
Pt_6O_3
Pt_6O_4
Pt_6O_5
Pt_6O_6
Pt_6O_7
Pt_6O_8
Pt_6O_9
Pt_6O_{10}
Pt_6O_{11}
Pt_6O_{12}

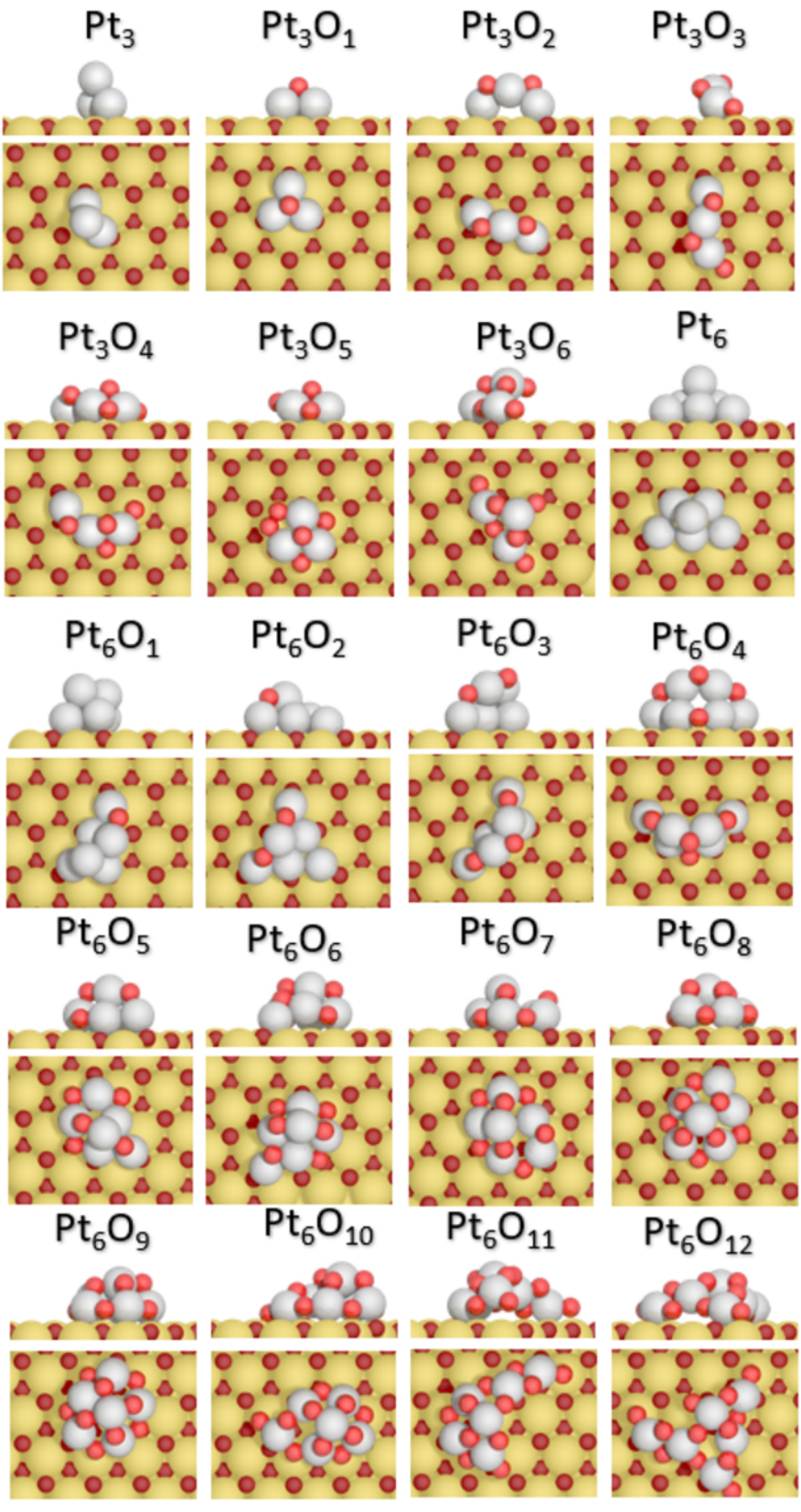
Pt_3
Pt_3O_1
Pt_3O_2
Pt_3O_3
Pt_3O_4
Pt_3O_5
Pt_3O_6
Pt_6
Pt_6O_1
Pt_6O_2
Pt_6O_3
Pt_6O_4
Pt_6O_5
Pt_6O_6
Pt_6O_7
Pt_6O_8
Pt_6O_9
Pt_6O_{10}
Pt_6O_{11}
Pt_6O_{12}

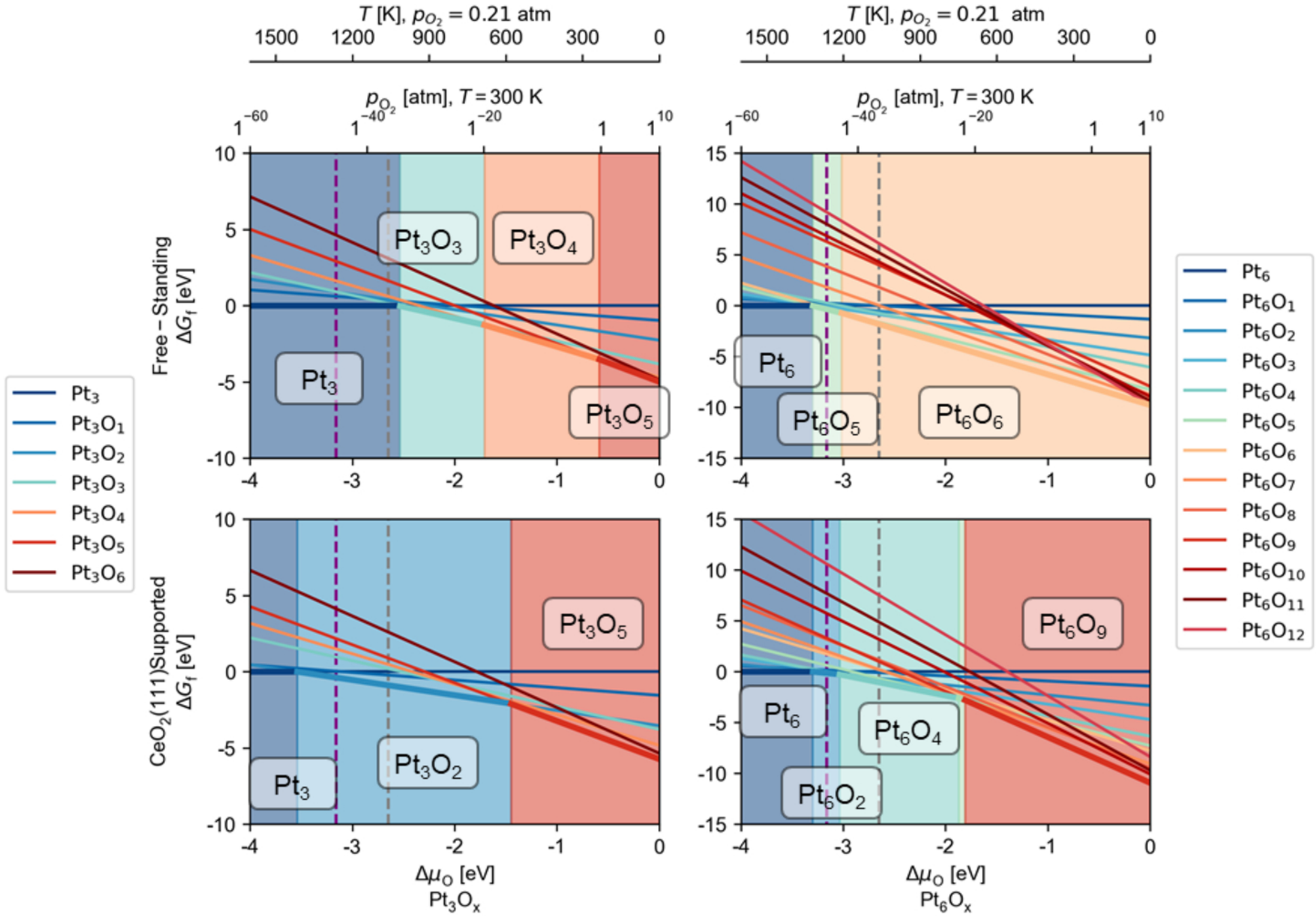
T [K], p_{O_2} = 0.21 atm
1500 1200 900 600 300 0
p_{O_2} [atm], T = 300 K
1^{-60} 1^{-40} 1^{-20} 1 1^{10}
Free – Standing ΔG_f [eV]
CeO_2(111)Supported ΔG_f [eV]
Pt_3
Pt_3O_1
Pt_3O_2
Pt_3O_3
Pt_3O_4
Pt_3O_5
Pt_3O_6
Pt_6
Pt_6O_1
Pt_6O_2
Pt_6O_3
Pt_6O_4
Pt_6O_5
Pt_6O_6
Pt_6O_7
Pt_6O_8
Pt_6O_9
Pt_6O_{10}
Pt_6O_{11}
Pt_6O_{12}
$\Delta\mu_O$ [eV]
Pt_3O_x
Pt_6O_x

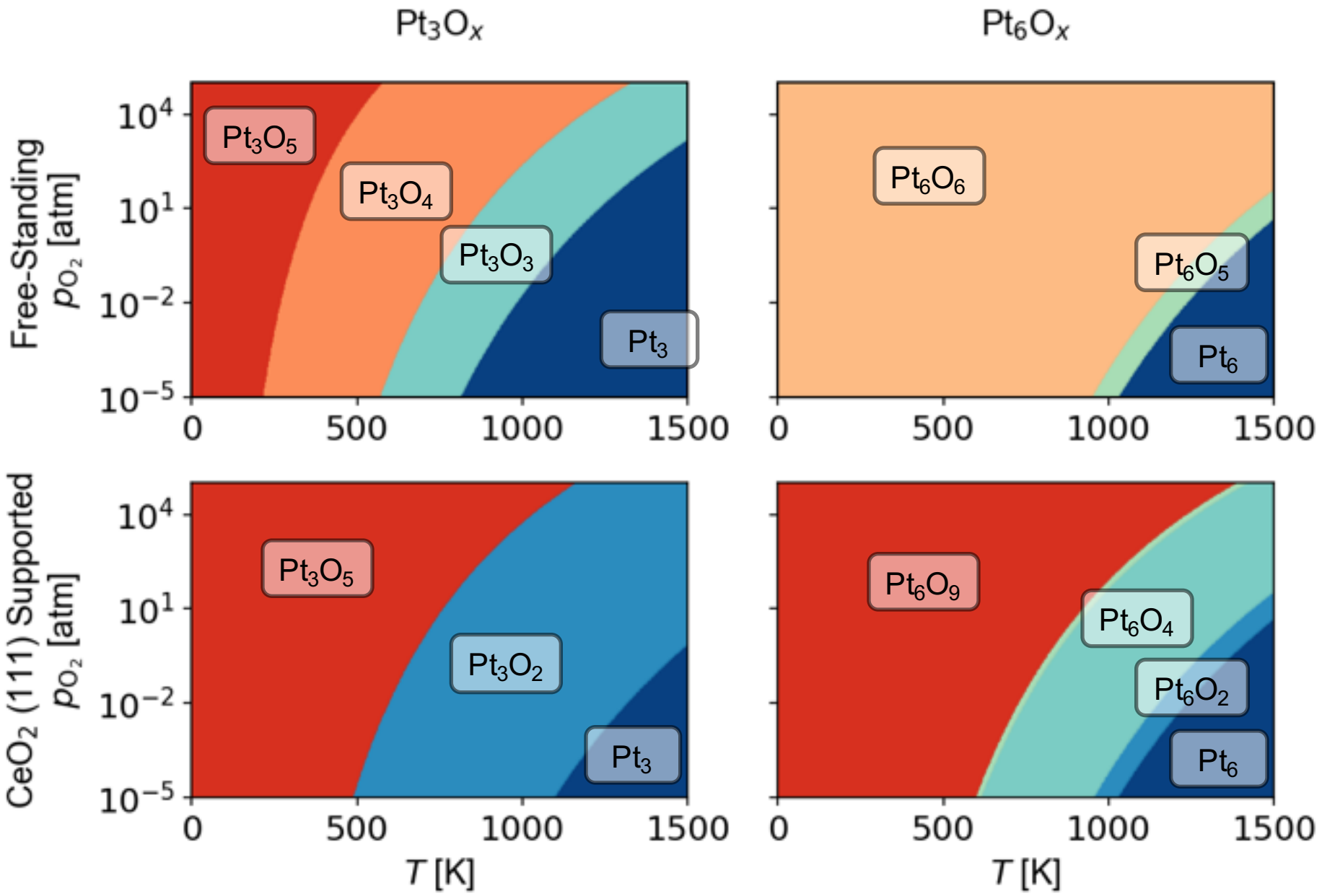
Pt_3O_x
Pt_6O_x
Free-Standing
p_{O_2} [atm]
CeO_2 (111) Supported
p_{O_2} [atm]
10^4
10^1
10^{-2}
10^{-5}
Pt_3O_5
Pt_3O_4
Pt_3O_3
Pt_3
Pt_6O_6
Pt_6O_5
Pt_6
Pt_3O_5
Pt_3O_2
Pt_3
Pt_6O_9
Pt_6O_4
Pt_6O_2
Pt_6
0
500
1000
1500
T [K]

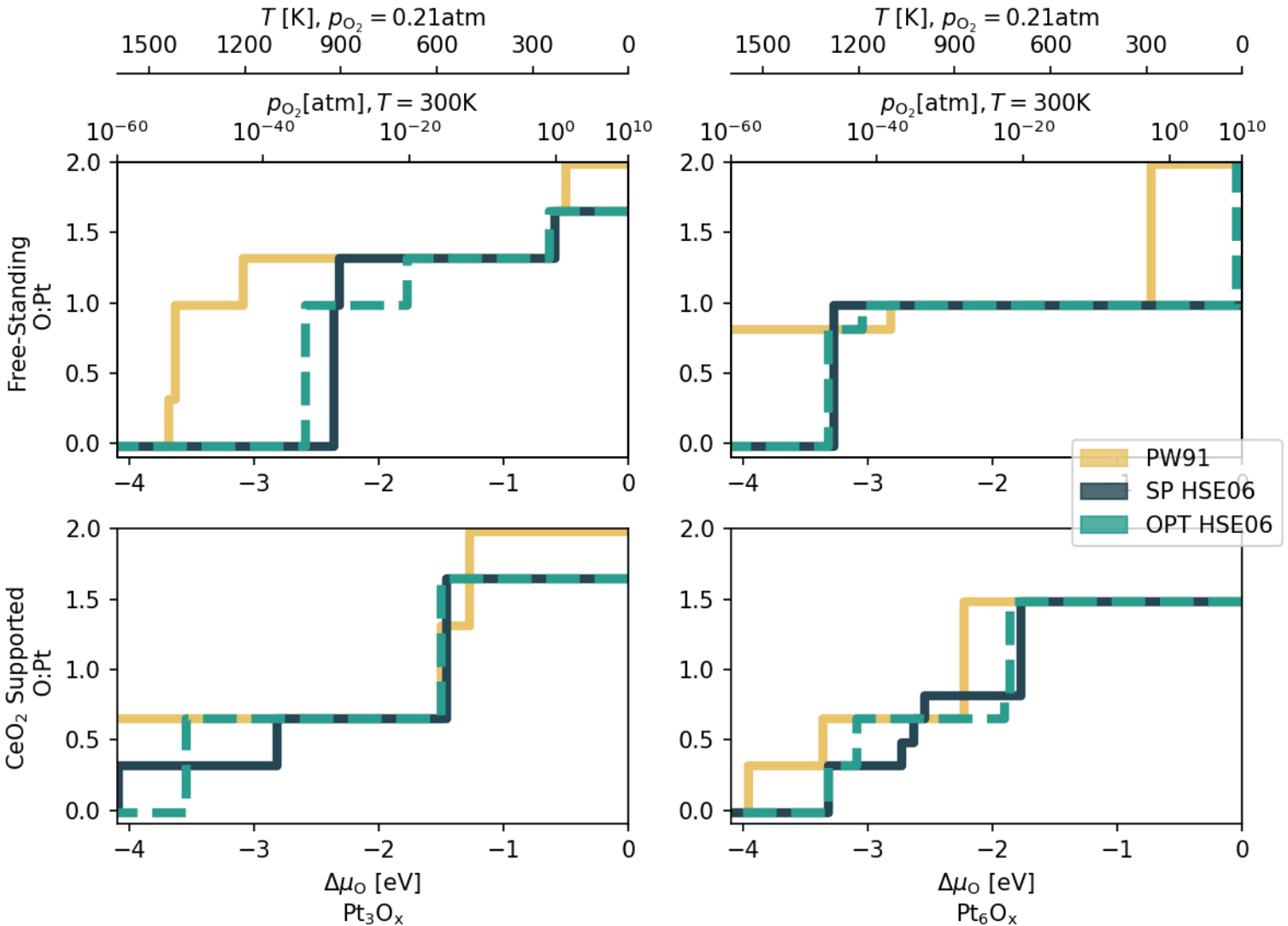
T [K], $p_{O_2} = 0.21$atm
1500
1200
900
600
300
0
p_{O_2}[atm], $T = 300$K
10^{-60}
10^{-40}
10^{-20}
10^{0}
10^{10}
Free-Standing
O:Pt
CeO_2 Supported
O:Pt
2.0
1.5
1.0
0.5
0.0
−4
−3
−2
−1
0
PW91
SP HSE06
OPT HSE06
$\Delta\mu_O$ [eV]
Pt_3O_x
Pt_6O_x

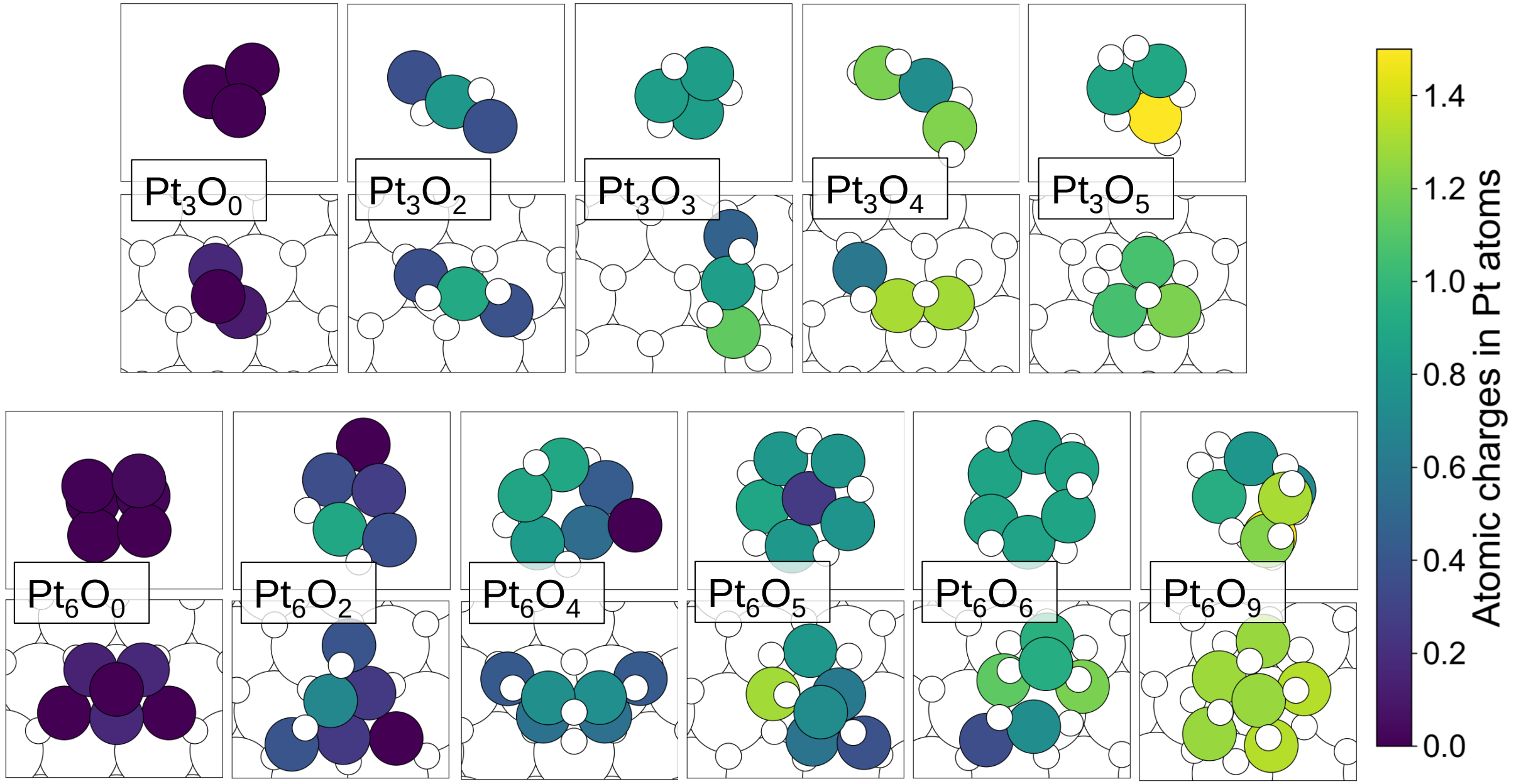
Pt_3O_0
Pt_3O_2
Pt_3O_3
Pt_3O_4
Pt_3O_5
Pt_6O_0
Pt_6O_2
Pt_6O_4
Pt_6O_5
Pt_6O_6
Pt_6O_9
Atomic charges in Pt atoms
0.0
0.2
0.4
0.6
0.8
1.0
1.2
1.4